UNIVERSITY OF BIRMINGHAM

University of Birmingham Research at Birmingham

Commercial SQUID magnetometer-compatible NMR probe and its application for studying a quantum magnet

Vennemann, Tarek; Jeong, Minki; Yoon, Dongyoung; Magrez, Arnaud; Berger, Helmuth; Yang, Lin; Zivkovic, Ivica; Babkevich, Peter; Rønnow, H. M.

Document Version
Peer reviewed version

[Link to publication on Research at Birmingham portal](#)

Note: Commercial SQUID magnetometer-compatible NMR probe and its application for studying a quantum magnet

T. Vennemann,[1] M. Jeong,[1, a)] D. Yoon,[2] A. Magrez,[3] H. Berger,[3] L. Yang,[1] I. Živković,[1] P. Babkevich,[1] and H. M. Rønnow[1, b)]

[1)]*Laboratory for Quantum Magnetism, Institute of Physics, Ecole Polytechnique Féderale de Lausanne (EPFL), CH-1015 Lausanne, Switzerland*

[2)]*Laboratory of the Physics of Nanostructured Materials, Institute of Physics, Ecole Polytechnique Féderale de Lausanne (EPFL), CH-1015 Lausanne, Switzerland*

[3)]*Crystal Growth Facility, Institute of Physics, Ecole Polytechnique Féderale de Lausanne (EPFL), CH-1015 Lausanne, Switzerland*

(Dated: 5 March 2018)

We present a compact NMR probe which is compatible with a magnet of a commercial SQUID magnetometer and demonstrate its application to the study of a quantum magnet. We employ trimmer chip capacitors to construct an NMR tank circuit for low temperature measurements. Using a magnetic insulator $MoOPO_4$ with $S = 1/2$ (Mo^{5+}) as an example, we show that the T-dependence of the circuit is weak enough to allow the ligand-ion NMR study of magnetic systems. Our ^{31}P NMR results are compatible with previous bulk susceptibility and neutron scattering experiments, and furthermore reveal unconventional spin dynamics.

Nuclear Magnetic Resonance (NMR) is a versatile tool for studying a wide variety of physical and chemical phenomena.[1] In particular, NMR is a powerful local probe of static and dynamic aspects of magnetism in solids, and has contributed critically to understanding magnetic and superconducting materials.[2] Although NMR is often regarded as a specialized technique requiring costly equipment, recent developments including FPGA(Field Programmable Gate Arrays)-based compact spectrometers and radio processors are lowering the barrier in terms of cost and instrument complexity.[3,4] Another source of large cost is a high-homogeneity superconducting magnet. However, for magnetism research with inhomogeneously broadened spectral lines, the high-homogeneity condition can be substantially relaxed.[5] This motivated us to use a magnet of a widely available, commercial SQUID (Superconducting Quantum Interference Device) magnetometer for NMR experiments. SQUID magnetometers can be expected to have a homogeneity of 100 ppm over 40 cm,[6] which amounts to a few tens of ppm for typical sample size of a few mm, and therefore provides enough resolution for inhomogeneously broadened NMR linewidths that easily exceed several hundreds of ppm.

The SQUID enables easy and precise measurements of bulk magnetic susceptibility. A great number of magnetism laboratories across the world are equipped with such instruments. However, it probes the bulk of a sample, providing only an averaged information. The spatially varying or local properties remain essentially inaccessible. An obvious example is an antiferromagnet where the stagerred magnetization averages out. Another frequent example would be a sample with a small amount of unwanted (quasi-)free magnetic impurities whose susceptibility diverges as T is lowered and which may well mask the intrinsic susceptibility. This further motivates us to install an NMR probe into the SQUID magnet,

which would allow us to track the intrinsic spin susceptibility,[7] enabling direct comparison with the bulk one.

In this Note, we present the construction of an NMR probe compatible with commercial SQUID magnetometers, specifically the model MPMS-5 of *Quantum Design Inc.*, and its successful application for investigating a quantum magnet. Our choice of material is a simple square-lattice quantum antiferromagnet $MoOPO_4$, being already characterized by a variety of experimental techniques,[8] which allows us a check of consistency.

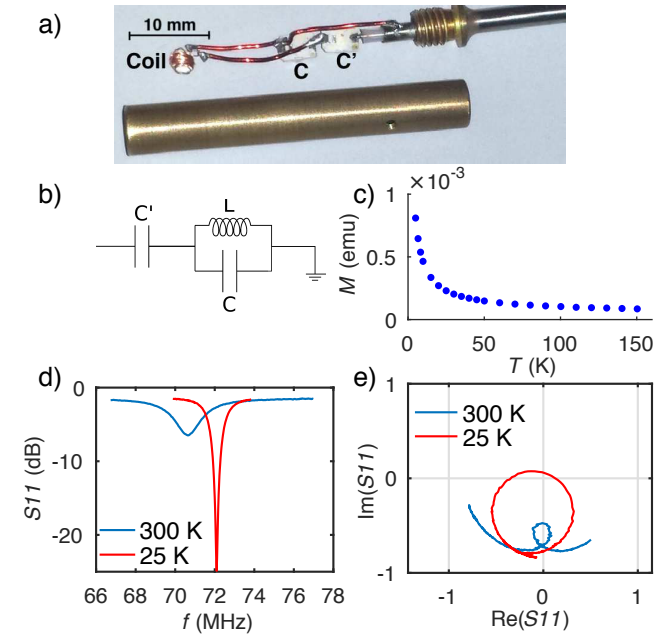FIG. 1. (a) Photograph of the NMR circuit and protective can. (b) NMR circuit diagram. (c) Magnetic moment of a chip capacitor as a function of T. (d) Resonance of the circuit at 300 and 25 K as observed in S_{11} and (e) its polar plot.

Figure 1(a) shows the NMR tank circuit built with a coil (L) and two trimmer chip capacitors, one for the resonant frequency tuning (C) and the other for impedance
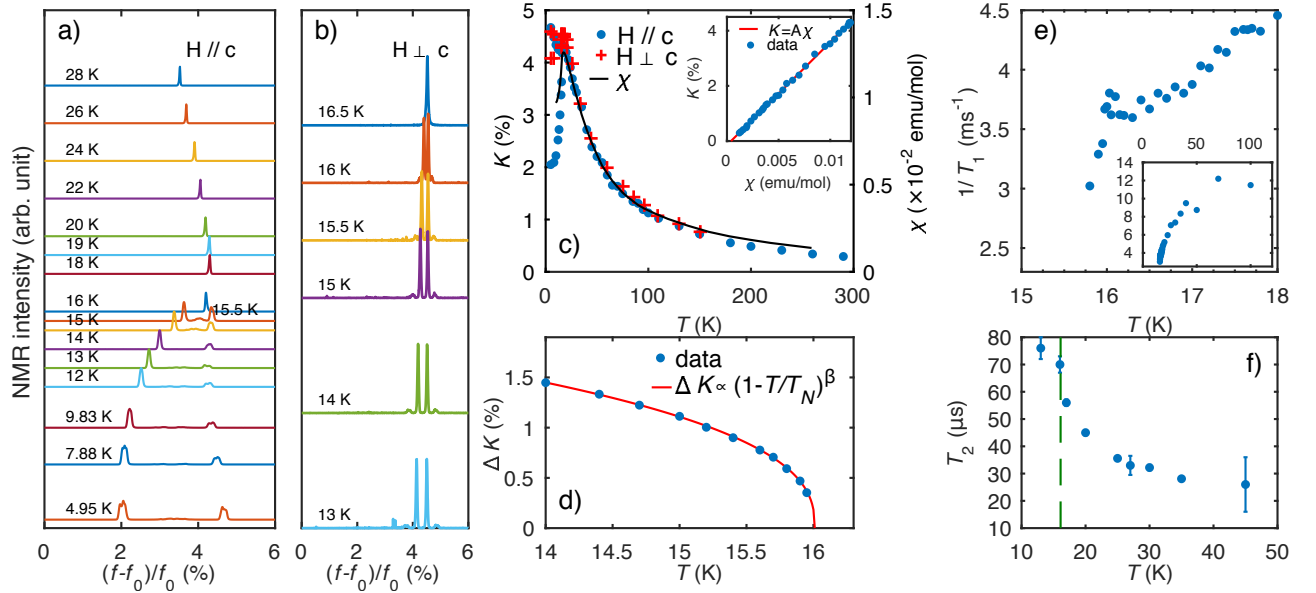

FIG. 2. (a) T-evolution of the ^{31}P NMR spectrum of MoOPO$_4$ in a magnetic field of 4 T applied along c axis and (b) perpendicular to c axis. (c) K as a function of T. Solid line shows bulk susceptibiltiy (right axis) measured by the SQUID, with the sample mounted into the NMR probe, in 4 T applied along the c axis. Inset shows K versus the bulk susceptibility for T-range 17-290 K. (d) The line splitting as a function of T near the magnetic transition for the field along the c axis. (e) $1/T_1$ as a function of T. Inset shows the data over the whole measurement region. (f) T_2 as a function of T.

matching (C'), and a shielding can. The corresponding circuit diagram of the series-parallel configuration[9] is shown in Fig. 1(b). We used *JZ060HV* and *JZ200HV* capacitors of *Voltronics Corp.*, having ranges of $C = 2\text{-}6$ pF and $C' = 4.5\text{-}20$ pF, respectively. Their dimensions are $4.5 \times 3.2 \times 1.5$ mm^3. For the target frequency around 70 MHz the coil was wound around the sample with 25 turns using a 0.1 mm in diameter copper wire; the coil had an oval-shaped cross section of about 3 mm by 1 mm.

The circuit is protected by the brass can which also provides shielding from external noise. Three small holes were made at the bottom and on the wall of the can to allow the He gas to flow through in order to efficiently cool and warm the sample within the VTI (Variable Temperature Insert) of the MPMS-5. The outer diameter of the can is 6 mm with a thickness of 1 mm, being slightly smaller than the inner diameter of 9 mm of the VTI sample space. Its length is 4 cm allowing for the sample to sit away from the capacitors. The stick part of the probe consists of a 1.3 m long hollow steel rod with an outer diameter of 3 mm in order to fit into the MPMS-5. Inside this rod is placed a 1.4 m long *UT85-SS-SS* semi-rigid coaxial cable from *micro-coax* of outer diameter 2.2 mm. At the top of the stick the coaxial cable protrudes by about 9 mm and is soldered to the hollow steel in an airtight way. It ends in a standard female SMA connector. At the bottom the circuit is soldered directly onto the coaxial cable, and the steel rod is soldered to a threaded brass piece onto which the can is screwed [Fig. 1(a)].

The radio-frequency pulse was generated by *SpinCore RadioProcessor* using *MXG Analog signal generator, Agilent*, as a continuous source and amplified by a 57 dB power amplifier *BT00500-Gamma, TOMCO Technologies*. The NMR signal from the probe was demodulated and then acquired using *Oscar Express 4427 CompuScope*

digitizer, *GaGe*. The mixing, modulation and demodulation was controlled by a home-built spectrometer.

Ideally the capacitors should not show any magnetism, but the ones used, made of a ceramic dielectric, show a slight magnetism. In Fig. 1(c) the magnetic moment as a function of T in an applied field of 500 Oe shows a Curie-like behavior with 8×10^{-4} emu at 5 K. However, the field they create at the sample location, about 1 cm away, is negligible. It only amounts to 0.1 Oe for an applied field of 500 Oe at 5 K. On the other hand, the T-dependence of the capacitance and resistance of the circuit impacts the conditions for NMR experiments more directly. Figure 1(d) shows the circuit resonance in terms of the reflection coefficient S_{11} against frequency at 300 and 25 K. The capacitance of each capacitor is adjusted at room temperature before closing the shielding can such that the circuit is intentionally under-matched and the resonance frequency lies somewhat below the target value. The S_{11} minimum corresponding to the resonance at 300 K is only about -5 dB but grows into a good matching of -25 dB at 25 K [see the polar plot in Fig. 1(e) as well]. The impedance at resonance (Z) was matched to a standard 50 Ω generator impedance. Z improved from $27.3 - 35.2\text{i}\ \Omega$ at 300 K to $51.6 + 5.6\text{i}\ \Omega$ at 25 K. The resonance frequency shifted from 70 MHz at 300 K to 72 MHz at 25 K, which was taken into account by changing the magnetic field accordingly, assuring that the measurement was always performed with a matched circuit.

Let us briefly outline the physical characteristics of MoOPO$_4$ that features a J_1-J_2 Heisenberg model with $S = 1/2$ (Mo^{4+}) on a stacked square lattice of a tetragonal structure. It undergoes an antiferromagnetic transition around $T_N = 16.1$ K, and the ground state is shown by neutron diffraction to have a Néel-type collinear staggered order (the ordered moments pointing parallel to the

crystallographic c axis) in the ab plane while the moments between the planes align themselves ferromagnetically. A spin-flop transition occurs around the applied field of 3.5 T for $H \parallel c$, but not for $H \perp c$, in the zero temperature limit. The spin-flop field increases up to 4.5 T with increasing T, terminated by the transition into a thermal paramagnet. We have chosen 4 T as a target field to explore both the collinear and spin-flopped phases while scanning T. This field value for ^{31}P nuclear spins with $\gamma/2\pi = 17.235$ MHz/T corresponds to about 70 MHz.

Now we present the NMR results obtained with the probe. The spectra and spin-spin relaxation times (T_2) were obtained using a spin-echo pulse sequence with a $\pi/2$ pulse length of 1-3 μs and a power of $\sim$15 W. The echo time τ was 10-40 μs for the spectra and 20-150 μs for T_2 measurements. It was shortened when T_2 was small to improve signal to noise ratio. The spin-lattice relaxation rate $1/T_1$ measurements were done using a saturation recovery, $\pi/2$-$\pi/2$-π sequence with waiting times after saturation of 4-5000 μs and echo times of 10-40 μs . Figures 2(a) and (b) show the T-evolution of the spectrum against reduced frequency $(f - f_0)/f_0$ with $f_0 = H\gamma/2\pi$, for $H \parallel c$ and $H \perp c$, respectively. In both cases, one observes that a single NMR line at high T splits into two well-separated lines as T is decreased across T_N. This signifies the appearance of two magnetic sublattices and thus the staggered antiferromagnetic order,[10] being consistent with the neutron diffraction results.[8] Figure 2(c) plots the fractional NMR line shift $K = (f_{res} - f_0)/f_0$ against T. Its inset shows K versus the bulk susceptibility (χ) from an independent SQUID measurement. K and χ show excellent agreement with a linear relation at T above T_N, from which we extracted the transferred hyperfine constant $A = 2.1$ T/μ_B between the Mo^{4+} and ^{31}P nuclei. In addition, we find that the splitting for $H \parallel c$ follows a power-law behavior near T_N, as shown in Fig. 2(d), where the obtained critical exponent $\beta = 0.39 \pm 0.02$, being compatible with a 3D Heisenberg model,[11] is larger than the value of 0.23 obtained from the neutrons.[8] However, a meaningful comparison would require more data points in the vicinity of T_N and more careful analysis, e.g., substraction of critical fluctuations from the neutron magnetic Bragg intensities.[8]

$1/T_1$ decreases monotonically with lowering T, followed by a tiny peak at T_N, as can be seen in Figure 2(e). We note that these two observations are rather atypical. As the measured T range extends more than an order of magnitude higher than T_N or the Weiss temperature of 4-6 K,[8] one would expect a motionally narrowed, T-invariant $1/T_1$ in the high temperature limit, [12] unlike our observation. In addition, the peak is heavily suppressed[13] compared to the ones ordinarily observed for an antiferromagnetic transition.[14] Nevertheless, they

may be consistent with each other: the antiferromagnetic correlations develop over a wide T range and thus little correlations would remain to be developed at the transition. T_2, shown in Figure 2(f), further corroborates the unconventional spin dynamics by showing a smooth increase[15] across the transition in contrast to the ordinary case of a sharp decrease.[14] We leave a detailed study of this unconventional dynamics for future work.

The same probe can be used to measure the bulk susceptibility of the sample while inside the SQUID magnetometer. It is then better to avoid using magnetic coax cables or capacitors. However, even if the cable and capacitors show slight magnetism, one can use background subtraction from the dipole curve to deduce the sample susceptibility. Figure 2(c) shows the thus-obtained susceptibility of the sample mounted in the NMR circuit.

To summarize, we have shown that one can easily install an NMR probe for the investigation of quantum magnets into the magnet of a commercial, widely-available SQUID magnetometer. This capability allows to readily measure the intrinsic susceptibility and compare it with the bulk one from the SQUID measurement.

[1] M. H. Levitt, *Spin dynamics: basics of nuclear magnetic resonance* (John Wiley & Sons, 2001).

[2] H. Alloul, Scholarpedia **9**, 32069 (2014).

[3] K. Takeda, Rev. Sci. Instrum. **78**, 033103 (2007).

[4] M. Pikulski, T. Shiroka, H.-R. Ott, and J. Mesot, Rev. Sci. Instrum. **85**, 093906 (2014).

[5] C. Berthier, M. Horvatić, M.-H. Julien, H. Mayaffre, and S. Krämer, Comptes Rendus Physique **18**, 331 (2017).

[6] J. Clarke and A. I. Braginski, *The SQUID Handbook: Applications of SQUIDs and SQUID Systems*, Vol. 2 (John Wiley & Sons, 2006) p. 398.

[7] A. Olariu, P. Mendels, F. Bert, F. Duc, J. Trombe, M. De Vries, and A. Harrison, Phys. Rev. Lett. **100**, 087202 (2008).

[8] L. Yang, M. Jeong, P. Babkevich, V. M. Katukuri, B. Náfrádi, N. E. Shaik, A. Magrez, H. Berger, J. Schefer, E. Ressouche, M. Kriener, I. Živković, O. V. Yazyev, L. Forró, and H. M. Rønnow, Phys. Rev. B **96**, 024445 (2017).

[9] E. Fukushima and S. B. Roeder, *Experimental pulse NMR: a nuts and bolts approach* (Addison-Wesley Reading, MA, 1981).

[10] H. Ishikawa, N. Nakamura, M. Yoshida, M. Takigawa, P. Babkevich, N. Qureshi, H. M. Rønnow, T. Yajima, and Z. Hiroi, Phys. Rev. B **95**, 064408 (2017).

[11] M. Campostrini, M. Hasenbusch, A. Pelissetto, P. Rossi, and E. Vicari, Phys. Rev. B **65**, 144520 (2002).

[12] T. Moriya, Prog. Theor. Phys **16**, 23 (1956).

[13] M. Jeong, F. Bert, P. Mendels, F. Duc, J. Trombe, M. De Vries, and A. Harrison, Phys. Rev. Lett. **107**, 237201 (2011).

[14] M. Yoshida, M. Takigawa, H. Yoshida, Y. Okamoto, and Z. Hiroi, Phys. Rev. Lett. **103**, 077207 (2009).

[15] M. Belesi, I. Rousochatzakis, H. Wu, H. Berger, I. Shvets, F. Mila, and J.-P. Ansermet, Phys. Rev. B **82**, 094422 (2010).